JOC The Journal of Organic Chemistry

pubs.acs.org/joc Article

Successive Diels–Alder Cycloadditions of Cyclopentadiene to [10]CPP⊃C_{60}: A Computational Study

Gerard Pareras, Sílvia Simon, Albert Poater,* and Miquel Solà*

Cite This: J. Org. Chem. 2022, 87, 5149–5157 Read Online

ACCESS | Metrics & More | Article Recommendations | Supporting Information

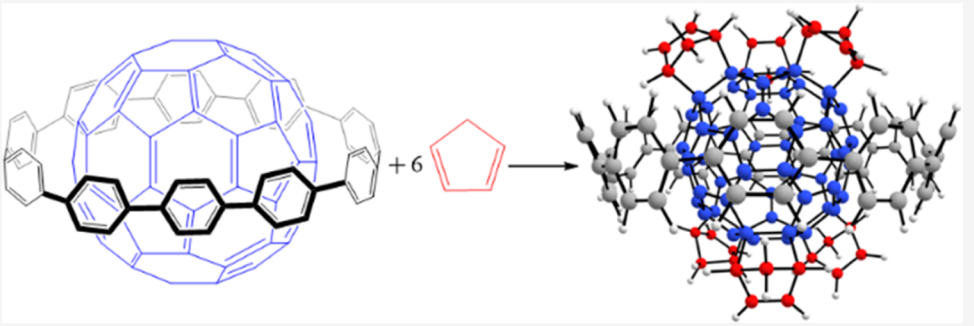

ABSTRACT: Fullerenes have potential applications in many fields. To reach their full potential, fullerenes have to be functionalized. One of the most common reactions used to functionalize fullerenes is the Diels–Alder cycloaddition. In this case, it is important to control the regioselectivity of the cycloaddition during the formation of higher adducts. In C_{60}, successive Diels–Alder cycloadditions lead to the T_h-symmetric hexakisadduct. In this work, we explore computationally using density functional theory (DFT) how the presence of a [10]cycloparaphenylene ring encapsulating C_{60} ([10]CPP⊃C_{60}) affects the regioselectivity of multiple additions to C_{60}. Our results show that the presence of the [10]CPP ring changes the preferred sites of cycloaddition compared to free C_{60} and leads to the formation of the tetrakisadduct. Somewhat surprisingly, our calculations predict formation of this particular tetrakisadduct to be more favored in [10]CPP⊃C_{60} than in free C_{60}.

INTRODUCTION

Potential applications of fullerenes range from materials science (molecular switching devices, magnetic materials, and photovoltaics) to medicinal chemistry.[1−10] To increase their applicability, fullerenes have to be functionalized.[11] For instance, the use of C_{60} in molecular heterojunction dye-sensitized solar cells requires to attach a donor group to C_{60} to generate a donor–acceptor (D–A) dyad.[12−14] Cycloaddition reactions like the [4 + 2] Diels–Alder (DA) cycloadditions,[15,16] the [3 + 2] Prato reactions,[17,18] the Bingel cyclopropanations,[19] or the [2 + 2 + 2] cycloadditions,[20] among others, are efficient ways to functionalize fullerenes in a regioselective[11] and, in some cases, enantioselective manner.[21,22]

C_{60} has two types of bonds, namely, the pyracylenic type-[6,6] bond in the ring junction of two fused six-membered rings (six-MRs) and the corannulenic [5,6] bond in the ring junction between five- and six-MRs. Most cycloaddition reactions in empty fullerenes take place in the [6,6] bonds,[23,24] whereas in endohedral fullerenes, the preference for [6,6] or [5,6] bonds is less clear.[25−29]

Multiple additions to the fullerene cages are also possible depending on the conditions of the reaction.[30−32] They proceed with a high control of the regioselectivity during the formation of higher adducts. For instance, multiple DA cycloadditions to C_{60} can generate bisadducts, trisadducts, and so on, up to six consecutive additions to finally produce the pseudooctahedral T_h-symmetric hexakisadduct.[33−35] These multiple DA cycloadditions occur exclusively to the [6,6] bonds of C_{60}. In some cases, formed cycloadducts are thermally unstable and can undergo cycloreversion.[35]

In a previous computational study, Solà et al.[36] discussed the formation of the T_h-symmetric hexakisadduct through multiple DA cycloadditions of 1,3-butadiene to [6,6] bonds of C_{60}, concluding that during the successive addition processes enthalpy barriers slightly increase and the exothermicity of the cycloadditions diminishes. In addition, the authors reported that addition of an extra 1,3-butadiene to the hexakisadduct is not possible due to the high energy barrier that has to be surpassed.[36] Similar results were obtained by Das

Received: December 24, 2021
Published: March 23, 2022

https://doi.org/10.1021/acs.joc.1c03116
J. Org. Chem. 2022, 87, 5149–5157

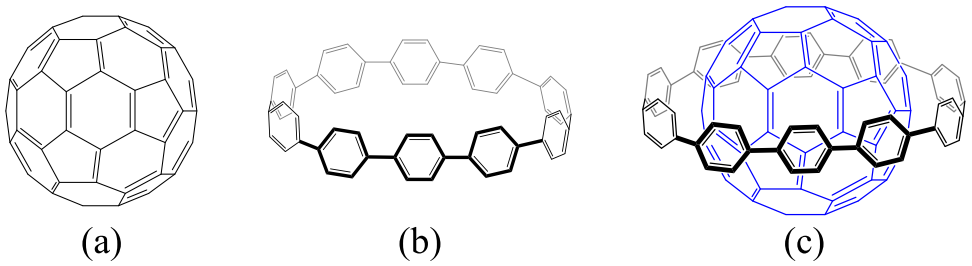

Figure 1. Structures of (a) C_{60}, (b) [10]CPP ring ($C_{60}H_{40}$), and (c) [10]CPP⊃C_{60}.

et al. in the successive DA cycloadditions of 1,3-butadiene to the [6,6] bonds of C_{60} and $Li^+@C_{60}$.[37]

[n]Cycloparaphenylenes ([n]CPPs) are hoop-shaped π-conjugated molecules in which the n paraphenylene units form a cycle.[38−40] These molecules can act as hosts for fullerenes (see Figure 1).[41,42] Yamago et al.[43,44] in 2011 proved that C_{60} can be selectively encapsulated by [10]CPP forming a stable [10]CPP⊃C_{60} system with a binding constant of $(2.79 \pm 0.03) \times 10^6$ L mol^{-1} in toluene. This [10]CPP⊃C_{60} system can act as a D−A dyad in which the charge-transfer process forms the [10]CPP^+⊃C_{60}^- system.[45] A similar charge-transfer process is observed in [10]CPP⊃$(C_{59}N)_2$⊂[10]CPP, a bis(azafullarene) $(C_{59}N)_2$ system complexed by two [10]CPP. The first [10]CPP macrocycle stabilizes the binding of the second by maximizing $\pi-\pi$, CH−π, and attractive London dispersion interactions.[46] Same type of interactions are key in the synthesis of [10]cycloparaphenylene-fullerene [2]rotaxanes[47] and in the recently synthesized figure-of-eight nanohoop that forms peanut-like 1:2 host−guest complexes with C_{60} or C_{70}.[48]

Very recently, Ribas et al.[49] reported the synthesis of a three-shell, matryoshka-like complex in which C_{60} inside a [10]CPP is in turn encapsulated inside a self-assembled nanocapsule. Bingel cyclopropanation to this matryoshka-like complex leads to the selective formation of a particular fullerene bisadduct. They also discussed how [n]CPPs can be used in combination with nanocages to purify and regioselectively functionalize fullerenes and endohedral metallofullerenes.[50] Inspired by these results, the main goal of the present work is to computationally investigate how the presence of the [10]CPP ring encapsulating C_{60} ([10]CPP⊃C_{60}) affects the regioselectivity of successive DA cycloadditions of cyclopentadiene to C_{60}. We anticipate here that our results show that in the presence of the [10]CPP, the pentakis and hexakisadducts of C_{60} are not formed.

RESULTS AND DISCUSSION

In the optimized [10]CPP⊃C_{60} species, the [10]CPP ring is located in the equator of C_{60} where the $\pi-\pi$ interactions are more favorable, dividing C_{60} into two equal poles. As mentioned before, in the DA reaction, the cyclopentadiene will attack the [6,6] bonds. We have assumed that the attacks occur sequentially over the freest [6,6] bonds. Considering that the equatorial plane (where the [10]CPP ring is located) is the most hindered region of C_{60} and taking into account the existence of two well-defined poles, we have assumed that additions of the second, fourth, and sixth cyclopentadiene will happen exactly in the same position of first, third, and fifth but on the opposite pole, i.e., path 4 → 4-4′ → 4-4-5 → 4-4′-5-5′→ 4-4′-5-5′-6 → 4-4′-5-5′-6-6′ (see Scheme 1 bottom). For the bisaddition, we also considered formation of the 4-5′ and 4-6′ bisadducts. These two bisadducts are the main products of the Bingel−Hirsch bisaddition to [10]CPP⊃C60 species.[51] Results given in Table S1 of the SI indicate that the 4-4′ DA bisadduct is about 2 kcal/mol more stable than the 4-5′ and 4-6′ and that the Gibbs energy barrier for the DA leading to the 4-4′ bisadduct is at least 2 kcal/mol lower than that generating the 4-5′ and 4-6′ bisadducts. Therefore, bisadducts 4-5′ and 4-6′ can be discarded as the main outcome in this DA bisaddition. Moreover, for each addition, there are two possible cycloadducts that correspond to the usual *endo* and *exo* attacks in DA cycloadditions. For all DA cycloadditions to [10]CPP⊃C_{60}, we have considered the two possible attacks and we report here only the attack with the lowest Gibbs reaction energy. On the other hand, for the addition to free C_{60}, we have followed the addition path 1 → 1-1′ → 1-1′-2 → 1-1′-2-2′ → 1-1′-2-2′-3 → 1-1′-2-2′-3-3′ (see Scheme 1 top), which is the thermodynamically most favorable according to Solà et al.[36]

Scheme 1. Top. Path Followed When Performing the Six Different Cycloadditions in Free C_{60} to Reach the T_h Hexakisadduct. Bottom. Path Followed When Performing the Six Different Cycloadditions in [10]CPP⊃C_{60} to Reach the C_{2h} Hexakisadduct

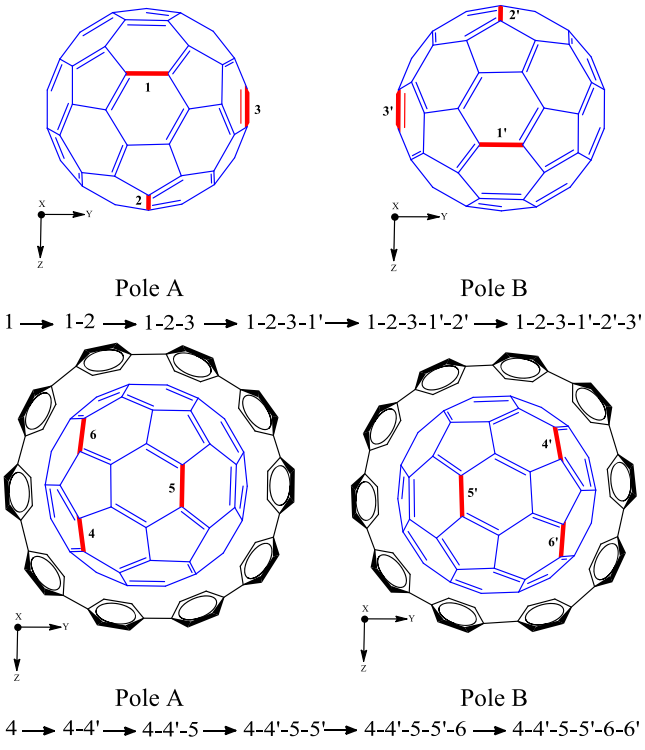

https://doi.org/10.1021/acs.joc.1c03116
J. Org. Chem. 2022, 87, 5149−5157

The DA cycloaddition of cyclopentadiene to [10]CPP⊃C_{60} starts with the formation of a reactant complex (RC) where the cyclopentadiene weakly interacts with [10]CPP⊃C_{60}, followed by the transition state (TS) of the [6,6]-attack, and finally, the product with the cyclopentadiene already attached to [10]-CPP⊃C_{60}. The first addition of the cyclopentadiene is considered to happen on the [6,6] bond at the very top of the C_{60} cage, being this position the freest as it is the one located furthest from the [10]CPP ring (see Figure 2). The

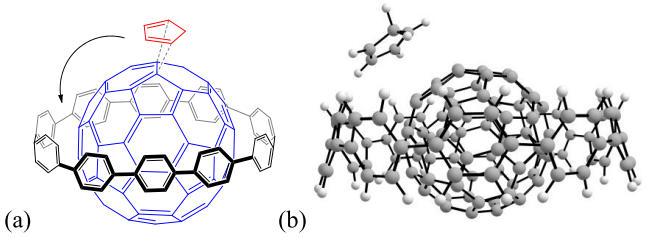

Figure 2. (a) Representation of the rotation produced during the optimization of the first reactant complex and (b) final optimized geometry of the first reactant complex.

reaction mechanism under the study begins with the RC where the cyclopentadiene interacts weakly with the [10]CPP⊃C_{60}. In the RC formed, the cyclopentadiene not only interacts with C_{60} but also with the [10]CPP ring. The optimized geometry for the RC of the first insertion shows how C_{60} and cyclopentadiene rotate until the cyclopentadiene is interacting with both C_{60} and the [10]CPP unit to maximize dispersion interactions (see Figure 2). Indeed, the four first additions occur close to the [10]CPP ring (Figure 3), which stabilizes RCs and TSs through dispersion interactions (vide infra).

Consecutively, the second insertion will happen on the same [6,6] bond but on the opposite pole. The methodology followed to study the subsequent cycloadditions is the same as for the first two insertions. Figure 3 collects the six products obtained by successive cycloadditions until the hexakisadduct is formed. The attacked positions differ from the ones attacked in free C_{60} (see Scheme 1).[36] In the following sections, we discuss in terms of energy values the path followed until the hexakisadduct is generated as well as the role of the [10]CPP ring over this process. For the sake of comparison, we also study the same DA cycloadditions on the same [6,6] bonds of the free C_{60} system without the [10]CPP ring.

Table 1 collects relative enthalpies and Gibbs energies of the RCs, TSs, and products of the different successive cycloadditions leading to the formation of the C_{2h} hexakisadduct system in [10]CPP⊃C_{60}. Both sets of relative energy values are also represented in the energy profiles of Figures 4 and 5.

Table 2 lists the activation energies and reaction energies derived from the enthalpies and Gibbs energies of Table 1. Enthalpies and Gibbs energies provide different trends. As to enthalpies, we find that reaction enthalpies are exothermic for all additions. After each addition, the individual enthalpy barriers (enthalpy difference between RC and TS) collected in Table 2 increase, whereas the exothermicity of the reaction decreases (same observations were made by Solà et al.[36] when discussing the formation of the T_h hexakisadduct in C_{60}). Although the first insertion needs to overcome an enthalpy barrier of only 12.8 kcal/mol, the last one requires 18.5 kcal/mol, an increase of around 6 kcal/mol (see Table 2). Reaction enthalpies decrease from −10.4 kcal/mol in the first insertion until −1.6 kcal/mol in the last one.

Gibbs reaction energies and Gibbs energy barriers collected in Table 2 do not change their trends compared to enthalpies, although they are higher by roughly 5−6 kcal/mol. Not surprisingly for entropic reasons, the energy barrier increases and the exothermicity decreases when considering Gibbs energies. Although trends given by Gibbs energies are the same as enthalpies, i.e., we observe the same increase of the energy barriers and a decrease of the reaction energies with successive

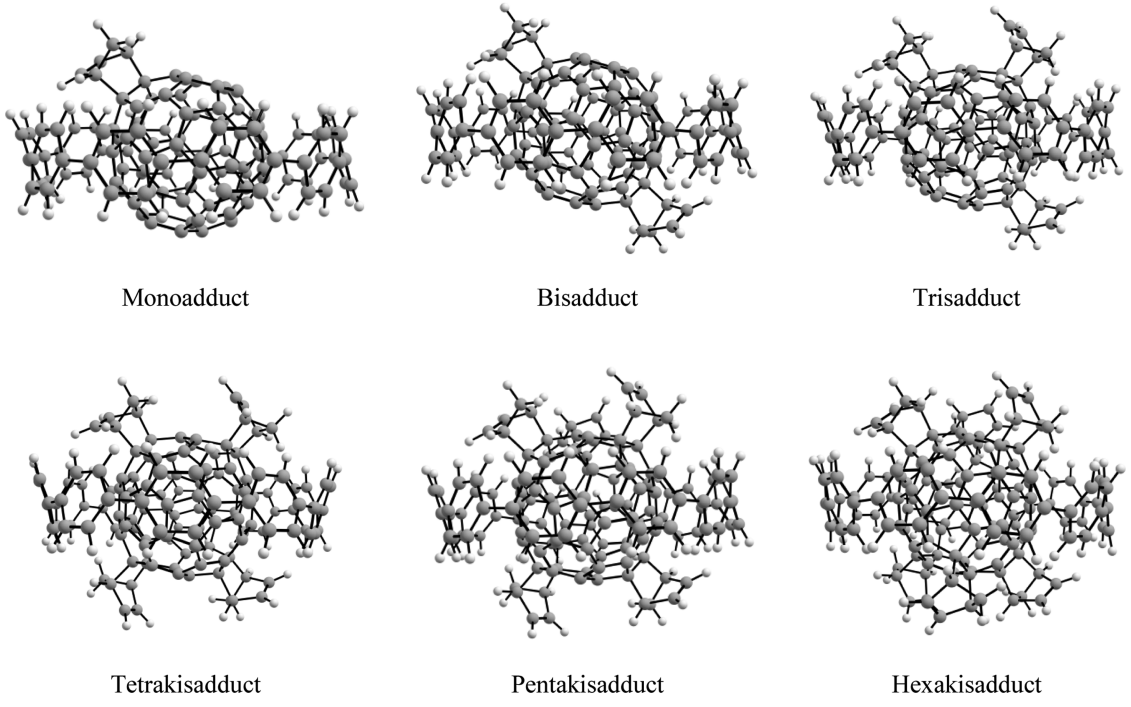

Figure 3. Optimized geometries of the [10]CPP⊃C_{60} products for the successive Diels−Alder reactions, from the first attack until the sixth.

https://doi.org/10.1021/acs.joc.1c03116
J. Org. Chem. 2022, 87, 5149−5157

Table 1. Relative Energy Values for All of the Reaction Steps Through the Six Cycloadditions, Collected Enthalpies, and Gibbs Energies (in kcal/mol) in Toluene Solution

structure[a]	ΔH	ΔG
[10]CPP⊃C_{60}+cyclopentadiene	0.00	0.00
RC 1[b]	−7.36	0.92
TS 1[c]	5.44	18.40
product 1	−17.79	−3.44
RC 2	−25.33	−2.52
TS 2	−12.10	15.28
product 2	−35.12	−6.38
RC 3	−42.63	−5.92
TS 3	−26.52	14.30
product 3	−48.69	−6.50
RC 4	−56.21	−6.06
TS 4	−39.82	14.56
product 4	−61.96	−6.30
RC 5	−68.46	−5.15
TS 5	−50.53	16.84
product 5	−70.49	−1.63
RC 6	−77.36	−1.44
TS 6	−58.88	21.71
product 6	−78.93	3.10

[a]Order of addition is 4 → 4-4′ → 4-4′-5 → 4-4′-5-5′ → 4-4′-5-5′-6 → 4-4′-5-5′-6-6′ (Scheme 1). [b]RC = Reactant complex. [c]TS = transition state.

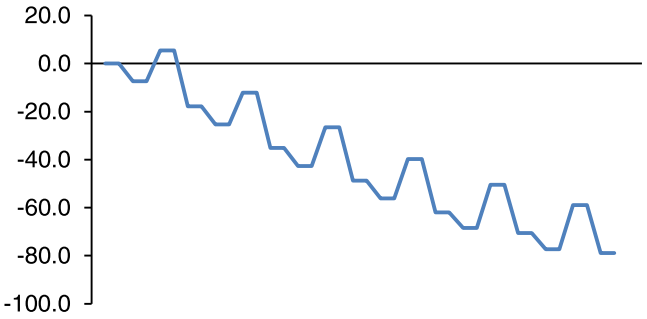

Figure 4. Enthalpy profile (kcal/mol) in toluene solution for the successive additions of cyclopentadiene to [10]CPP⊃C_{60}.

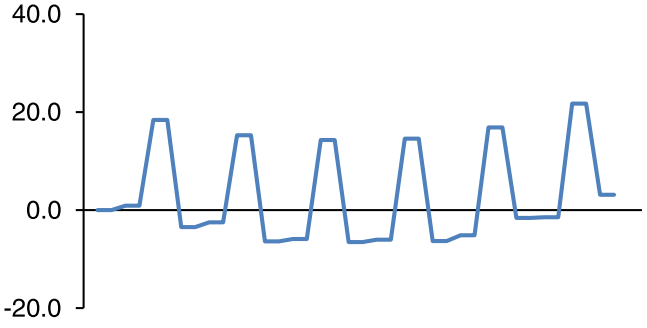

Figure 5. Gibbs energy profile (kcal/mol) in toluene solution for the successive additions of cyclopentadiene to [10]CPP⊃C_{60}.

additions, there are some relevant differences. The most important one is that Gibbs reaction energies reach positive values after the fourth insertion, indicating that the formation of pentakis- and hexakisadducts is not thermodynamically favored (see Figure 5) and can therefore be assumed that the reaction will stop on the tetrakisadduct system. However, we

Table 2. Activation Energies and Reaction Energies for Successive Additions to [10]CPP⊃C_{60}[a]

	enthalpy		Gibbs energy	
addition[b]	activation energy	reaction energy	activation energy	reaction energy
1	12.80	−10.43	17.48	−4.36
2	13.23	−9.79	17.79	−3.86
3	16.10	−6.06	20.23	−0.58
4	16.38	−5.75	20.62	−0.24
5	17.93	−2.04	21.98	3.52
6	18.48	−1.57	23.15	4.54

[a](Enthalpies and Gibbs Energies in kcal/mol) in Toluene Solution. [b]Order of addition is 4 → 4-4′ → 4-4-5 → 4-4′-5-5′ → 4-4′-5-5′-6 → 4-4′-5-5′-6-6′ (Scheme 1).

expect a complex equilibrium between reactants and the different possible products. In particular, because the Gibbs energies of the pentakis- and hexakisadducts are 3.5 kcal/mol and 4.5 kcal/mol above their respective reactant complexes and their relative Gibbs energies with respect to separated reactants are −1.6 and 3.1 kcal/mol, respectively, it is likely that if the DA cycloaddition is carried out in the presence of a large excess of cyclopentadiene the reaction could afford the formation of minor quantities of the pentakis- and hexakisadducts. The increase in the energy barriers with successive additions is attributed mainly to the increase of the lowest unoccupied molecular orbital (LUMO) energy of the fullerenic cage (vide infra).

To unveil the effect of the presence of the [10]CPP, the same attacks studied for the [10]CPP⊃C_{60} species have also been studied removing the [10]CPP unit.

For the sake of comparison, the energy profiles for the six cycloadditions to the same [6,6] bonds of C_{60} and [10]-CPP⊃C_{60} values have been compared in Figures 6 and 7. In

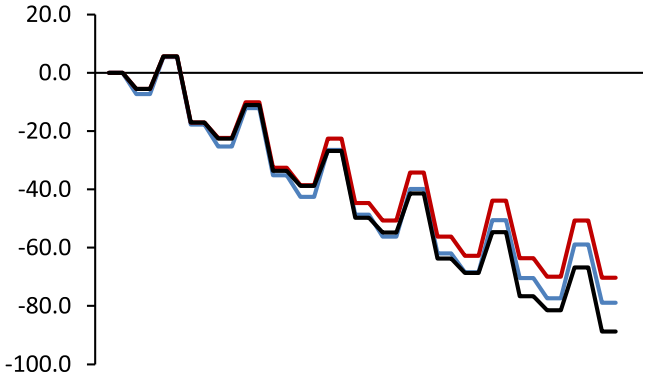

Figure 6. Enthalpy profile (kcal/mol) in toluene solution of the successive DA cycloadditions of cyclopentadiene to [10]CPP⊃C_{60} in blue color, C_{60} in red color, and C_{60} with the successive Diels−Alder cycloadditions studied by Solà et al.[36] in black color.

comparison with [10]CPP⊃C_{60} values, relative energies of all RC, TSs, and products are lower in [10]CPP⊃C_{60} as compared to C_{60} because of better dispersion interactions (see Table S2). In Table 3, the activation energies and reaction energies for each individual DA reaction are included. Pang and Wilson[52] found that the activation energy for the first DA reaction of C_{60} and cyclopentadiene in high-pressure liquid chromatography is 6.9 kcal/mol, whereas Giovane et al.[53] reported an activation energy of 26.7 ± 2.2 kcal/mol for the

https://doi.org/10.1021/acs.joc.1c03116
J. Org. Chem. 2022, 87, 5149−5157

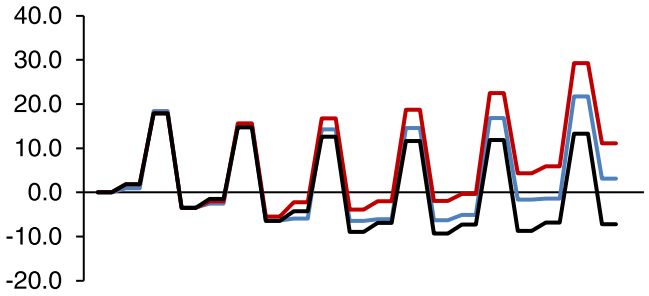

Figure 7. Gibbs energy profile (kcal/mol) in toluene solution of the successive DA cycloadditions of cyclopentadiene to [10]CPP⊃C_{60} in blue color, C_{60} in red color, and C_{60} with the successive Diels–Alder cycloadditions studied by Solà et al.[36] in black color.

Table 3. Activation Energies and Reaction Energies for Each Addition over the C_{60} Structure[a]

	enthalpy		Gibbs energy	
addition[b]	activation energy	reaction energy	activation energy	reaction energy
1	11.15	−11.60	16.04	−5.34
2	12.19	−10.27	17.67	−3.43
3	15.90	−6.15	18.98	−1.67
4	16.44	−5.59	20.69	0.03
5	18.89	−0.82	22.86	4.70
6	19.35	−0.31	23.39	5.23

[a](Enthalpies and Gibbs Energies in kcal/mol) in Toluene Solution. [b]Order of addition is 4 → 4-4′ → 4-4′-5 → 4-4′-5-5′ → 4-4′-5-5′-6 → 4-4′-5-5′-6-6′ (Scheme 1).

corresponding retro-DA cycloaddition in tetrachloroethane. From the combination of these two numbers, one can estimate the reaction energy to be −19.8 ± 2.2 kcal/mol. These experimental values have to be compared with the $\Delta H^{\ddagger}$ = 11.2 kcal/mol and ΔH_r = −11.6 kcal/mol obtained in our study (Table 3). These results show that our calculated activation energies may be somewhat overestimated and the reaction energies somewhat underestimated. On the other hand, Ueno et al.[34] found that the DA of 1,3-cyclohexadiene with C_{60} has an activation barrier of 16.1 kcal/mol in dichloromethane. Activation energies for the first additions over C_{60} are slightly lower than the activation energies for [10]CPP⊃C_{60}, whereas for additions 5–6 are somewhat higher. In detail, this difference is only about 1 kcal/mol for additions 1–3 in favor of C_{60}, while for additions 5 and 6, they are slightly higher for the C_{60} system, also around 1 kcal/mol. The fact that the fifth and sixth additions of cyclopentadiene to C_{60} are more favorable in [10]CPP⊃C_{60} than in pristine C_{60} is likely to be the result of an overestimation of the dispersion interactions by the D3(BJ) method. Reaction enthalpy values follow a similar trend, and thus, insertions 1 to 3 are less exothermic for [10]CPP⊃C_{60}. However, the two last insertions become more exothermic for [10]CPP⊃C_{60}. In general terms, although the differences found due to the presence of the [10]CPP are relatively small, the [10]CPP ring tends to difficult additions 1–3 and favor additions 4–6.

Gibbs energy values again show that the reaction would stop at insertions 3-4 resulting in the formation of the tris- and tetrakisadducts in equilibrium. Interestingly, the increase in the Gibbs energy barriers and the destabilization of the products after the third or fourth addition is greater for C_{60} than for [10]CPP⊃C_{60}. The higher destabilization for the last additions in C_{60} is due to the fact that the successive cycloadditions over the poles happen in a very reduced space. Surprisingly, this detrimental effect is less marked in [10]CPP⊃C_{60} despite one would expect a higher hindrance due to the presence of the [10]CPP ring, which should be translated into a destabilization of the TSs and final products. However, for the fifth and sixth additions, dispersion interactions previously discussed between the cyclopentadiene and the [10]CPP ring stabilize somewhat more the TSs than the RCs, favoring the additions to [10]CPP⊃C_{60} as compared to those to C_{60}. The final conclusion is that the multiple cycloadditions to [10]CPP⊃C_{60} will stop at the fourth addition for thermodynamic reasons and that a mixture of bis-, tris-, and tetrakisadducts will be generated according to our calculations. The exact product distribution will depend on the initial concentration of cyclopentadiene and [10]CPP⊃C_{60}. Let us mention here that the successive DA cycloadditions to free C_{60} do not follow the same path as in the case of [10]CPP⊃C_{60} (see Scheme 1). Following the most stable thermodynamic path according to the work by Solà et al.,[36] i.e., the path 1 → 1-1′ → 1-1′-2 → 1-1′-2-2′ → 1-1′-2-2′-3 → 1-1′-2-2′-3-3′ in Scheme 1, one finds that the formation of the T_h hexakisadduct is possible although the most stable cycloadduct is the pentakisadduct (see Tables S2, S3 and Figures 6 and 7).

To get a deeper insight into the successive DA cycloadditions to [10]CPP⊃C_{60} and C_{60}, the deformation and interaction energies have been studied for each RC and TS. One can consider the energy of a given complex as the sum of the deformation energy (energy required to deform the fragments to the geometry they have in the complex that is always positive) and interaction energy (energy usually released as a result of the interaction between deformed fragments in the formation of the complex). Deformation and interaction energies for the TSs of the cycloadditions to [10]CPP⊃C_{60} and C_{60} are collected in Table 4, whereas those

Table 4. Deformation and Interaction Energies (kcal/mol) in Toluene Solution of the Transition States of the Different Diels–Alder Cycloadditions of Cyclopentadiene to [10]CPP⊃C_{60} and C_{60}

[a]	[10]CPP⊃C_{60} transition states					C_{60} transition states				
addition	E_{def1}	E_{def2}	E_{def}	E_{int}	$E_{def+Eint}$	E_{def1}	E_{def2}	E_{def}	E_{int}	$E_{def+Eint}$
1	8.7	18.5	27.2	−22.5	4.7	7.5	18.2	25.8	−20.9	4.9
2	8.0	19.0	27.0	−22.1	4.9	7.8	18.8	26.6	−20.4	6.2
3	8.3	20.2	28.5	−20.5	8.1	8.1	19.8	27.9	−18.6	9.3
4	8.3	20.4	28.7	−20.4	8.3	8.3	19.9	28.2	−18.4	9.8
5	9.4	18.5	28.0	−17.2	10.8	8.2	19.1	27.4	−15.6	11.8
6	9.3	19.0	28.3	−17.4	10.9	8.3	19.4	27.7	−15.5	12.3

[a]Order of addition is 4 → 4-4′ → 4-4′-5 → 4-4′-5-5′ → 4-4′-5-5′-6 → 4-4′-5-5′-6-6′ (Scheme 1).

https://doi.org/10.1021/acs.joc.1c03116
J. Org. Chem. 2022, 87, 5149–5157

Table 5. HOMO, LUMO, and HOMO−LUMO Energy Gap in eV for All of the Reactant Complexes (RCs) in the Multiple DA Cycloadditions of Cyclopentadiene to [10]CPP⊃C_{60} and C_{60}[a]

	[10]CPP⊃C_{60}			C_{60}		
structure	HOMO	LUMO	H−L gap	HOMO	LUMO	H−L gap
[10]CPP⊃C_{60}/C_{60}	−5.4	−3.4	2.1	−6.3	−3.6	2.7
RC 1	−5.5	−3.3	2.1	−6.1	−3.5	2.5
RC 2	−5.4	−3.2	2.2	−5.9	−3.4	2.5
RC 3	−5.4	−3.1	2.3	−5.7	−3.3	2.4
RC 4	−5.2	−2.9	2.3	−5.4	−3.1	2.3
RC 5	−5.0	−2.7	2.3	−5.1	−2.8	2.3
RC 6	−4.8	−2.5	2.3	−4.9	−2.7	2.3

[a]HOMO energy of the cyclopentadiene is −5.8 eV.

of the RCs are given in the SI (Table S4). Two deformation energies have been considered, *i.e.*, the deformation of [10]CPP⊃C_{60} or C_{60} (E_{def1}) and the deformation of cyclopentadiene (E_{def2}), being the total deformation energy the sum of both individual deformation energies ($E_{def} = E_{def1} + E_{def2}$).

The deformation of the TSs observed in fragments 1 is mainly due to changes in the attacked [6,6] bond. In [10]CPP⊃C_{60}, this energy is slightly higher as the [10]CPP ring also shows a small deformation to allow the cyclopentadiene approximation. The main deformation is that of the cyclopentadiene; however, this is energetically similar for [10]CPP⊃C_{60} and C_{60} if we consider the same attacked bonds. The main difference between [10]CPP⊃C_{60} and C_{60} stems from the interaction energy, which is always around 2 kcal/mol more stable for the first one. As previously observed, the energy of the TSs increases after each addition. Thanks to the information in Table 4, this increase can be attributed to the fact that both systems have to be slightly more deformed and that the interaction energy is reduced after each addition. The increase of the energy barrier for successive cycloadditions is somewhat smoother for [10]CPP⊃C_{60} than for C_{60} (considering the same attacks) not because of the stabilization due to better $\pi(HOMO_{cyclopentadiene})$-$\pi^*(LUMO_{cage})$ (vide infra) but due to the dispersion interactions present in [10]CPP⊃C_{60} as compared to C_{60}.

Finally, the frontier molecular orbitals (HOMO and LUMO) have been also studied for each reaction step and for both systems. As already indicated by Solà et al.,[36] after each addition, LUMO orbitals become less stable explaining the increase of the energy barriers and the reduction of the reaction enthalpy. In both cases, highest occupied molecular orbital (HOMO) (located in the cyclopentadiene) and LUMO (located in the fullerenic cage) energy values become more positive as the cycloadditions proceed (see Table 5), obtaining less electrophilic and more stable products. The main difference between the two systems is that both HOMO and LUMO energies for [10]CPP⊃C_{60} structures have higher energies than C_{60} structures. Lower LUMO energies for C_{60} explain the lower barriers for the 1−3 additions. However, for the fourth and sixth additions, the lower barriers for [10]CPP⊃C_{60} can only be explained by the higher dispersion interactions present in [10]CPP⊃C_{60}, which are probably somewhat overestimated using the D3(BJ) method. Finally, one can observe that the HOMO−LUMO gap in [10]-CPP⊃C_{60} structures is more constant, starting from 2.1 eV in the [10]CPP⊃C_{60} geometry, and after the first adduct, all of the energy values oscillate between 2.2 and 2.3 eV. This trend is slightly different for C_{60}. In this case, the HOMO−LUMO gap is reduced from 2.7 eV in C_{60} to 2.3 eV in the sixth insertion.

CONCLUSIONS

We have studied the multiple Diels−Alder cycloadditions of cyclopentadiene to [10]CPP⊃C_{60}. The [10]CPP ring divides the C_{60} of [10]CPP⊃C_{60} into two identical poles and the cycloadditions take place only over the poles of [10]CPP⊃C_{60} because the hindrance generated by the [10]CPP ring disfavors cycloadditions in the equator. The preferred sites of cycloaddition change when going from C_{60} to [10]CPP⊃C_{60}. In C_{60}, the final hexakisadduct has pseudooctahedral T_h symmetry, whereas in [10]CPP⊃C_{60}, it has C_{2h} symmetry. In general, in successive additions, we have observed an increase in the energy barrier and a reduction in the exothermicity of the reaction. Based on Gibbs energies, we have determined that the formation of the [10]CPP⊃C_{60} pentakis- and hexakisadducts is thermodynamically unfavorable and can only be reached in minor quantities by adding an excess of cyclopentadiene. Our results favor the formation of the tris- and tetrakisadducts in [10]CPP⊃C_{60}, at the variance of free C_{60}, in which the formation of the pentakisadduct is thermodynamically favored. Analyzing the additions that lead to the C_{2h} symmetry hexakisadduct but without the [10]CPP ring, we have found that the formation of the tetrakis-, pentakis-, and hexakisadducts is more favored in [10]CPP⊃C_{60} than in free C_{60} because of dispersion interactions with the [10]CPP ring, which are slightly more intense in the TSs than in the RCs. Finally, frontier molecular orbitals show a decrease in the energy of the LUMO orbitals, explaining the increase of the energy barriers and the reduction of the reaction enthalpy after each addition.

COMPUTATIONAL DETAILS

Theoretical calculations were performed by means of the Gaussian16 software package.[55] Geometry optimizations and frequency calculations were carried out with the B3LYP hybrid functional[56−59] using the standard 6-31G*[60] together with the Grimme's dispersion D3 correction to the electronic energy with the Becke−Johnson (BJ) damping.[61] Dispersion corrections are essential for the study of chemical reactivity in fullerenes.[62] For single-point energy refinements, the same B3LYP functional was used with the 6-311G** basis set.[63] The ultrafine integration grid was employed in all calculations. To simulate solvent effects, calculations were carried out in toluene using the polarizable continuum model (PCM).[64,65] On top of the B3LYP-D3(BJ)/6-311G**(toluene)//B3LYP-D3(BJ)/6-31G* electronic energies, we added the B3LYP-

https://doi.org/10.1021/acs.joc.1c03116
J. Org. Chem. 2022, 87, 5149−5157

D3(BJ)/6-31G* thermal and entropy corrections obtained in the gas phase at 298.15 K and under atmospheric pressure conditions. It is likely that the errors in reaction energies for such a method are below 4 kcal/mol.[66,67] Still, to get the product distributions, the important quantities are $\Delta\Delta G$ for the different products. In this case, we expect an error in $\Delta\Delta G$ much lower, in the order of 1 kcal/mol.

■ ASSOCIATED CONTENT

Supporting Information

The Supporting Information is available free of charge at https://pubs.acs.org/doi/10.1021/acs.joc.1c03116.

Tables with reaction energies and energy barriers for the different bisadditions, comparison between [10]-CPP⊃C_{60} and C_{60} attacks, and deformation energies. All XYZ coordinates and absolute energies of all computed species (PDF)

■ AUTHOR INFORMATION

Corresponding Authors

Albert Poater − *Institut de Química Computacional i Catàlisi and Departament de Química, Universitat de Girona, 17003 Girona, Catalonia, Spain;* orcid.org/0000-0002-8997-2599; Email: albert.poater@udg.edu

Miquel Solà − *Institut de Química Computacional i Catàlisi and Departament de Química, Universitat de Girona, 17003 Girona, Catalonia, Spain;* orcid.org/0000-0002-1917-7450; Email: miquel.sola@udg.edu

Authors

Gerard Pareras − *Institut de Química Computacional i Catàlisi and Departament de Química, Universitat de Girona, 17003 Girona, Catalonia, Spain; School of Chemistry, University College Cork, T12 YN60 Cork, Ireland*

Sílvia Simon − *Institut de Química Computacional i Catàlisi and Departament de Química, Universitat de Girona, 17003 Girona, Catalonia, Spain*

Complete contact information is available at: https://pubs.acs.org/10.1021/acs.joc.1c03116

Notes

The authors declare no competing financial interest.

■ ACKNOWLEDGMENTS

A.P. is a Serra Húnter Fellow and ICREA Academia Prize 2019. A.P., S.S,and M.S. thank the Spanish MINECO for projects PGC2018-097722-B-I00 and PID2020-13711GB-I00 and the Generalitat de Catalunya for project 2017SGR39. The work was performed under the Project HPC-EUROPA3 (HPC17870HV), with the support of the EC Research Innovation Action under the H2020 Programme. G.P. gratefully acknowledges the support of Institut de Química Computacional i Catàlisis (IQCC) and the computer resources and technical support provided by the Barcelona Supercomputing Center (CNS-BSC) and the Irish Centre for High-End Computing (ICHEC). Open Access funding provided thanks to the CRUE-CSIC agreement with ACS.

■ REFERENCES

(1) Guldi, D. M.; Martín, N. *Fullerenes: From Synthesis to Optoelectronic Properties*; Kluver: Dordrecht, 2002.

(2) De La Puente, F. L.; Nierengarten, J.-F. *Fullerenes: Principles and Applications*; RSC: Cambridge, 2011.

(3) Thilgen, C.; Diederich, F. Structural Aspects of Fullerene Chemistry - A Journey through Fullerene Chirality. *Chem. Rev.* **2006**, *106*, 5049−5135.

(4) Liu, J.; Qiu, L.; Shao, S. Emerging Electronic Applications of Fullerene Derivatives: An Era beyond OPV. *J. Mater. Chem. C* **2021**, *9*, 16143−16163.

(5) Li, J.; Chen, L.; Su, H.; Yan, L.; Gu, Z.; Chen, Z.; Zhang, A.; Zhao, F.; Zhao, Y. The Pharmaceutical Multi-Activity of Metallofullerenol Invigorates Cancer Therapy. *Nanoscale* **2019**, *11*, 14528−14539.

(6) Markovic, Z.; Trajkovic, V. Biomedical Potential of the Reactive Oxygen Species Generation and Quenching by Fullerenes (C_{60}). *Biomaterials* **2008**, *29*, 3561−3573.

(7) Izquierdo, M.; Platzer, B.; Stasyuk, A. J.; Stasyuk, O. A.; Voityuk, A. A.; Cuesta, S.; Solà, M.; Guldi, D. M.; Martín, N. All-Fullerene Electron Donor−Acceptor Conjugates. *Angew. Chem. Int. Ed.* **2019**, *58*, 6932−6937.

(8) Osuna, S.; Swart, M.; Solà, M. On the Mechanism of Action of Fullerene Derivatives in Superoxide Dismutation. *Chem. - Eur. J.* **2010**, *16*, 3207−3214.

(9) Li, W.; Wang, C.; Wang, T. Molecular Structures and Magnetic Properties of Endohedral Metallofullerenes. *Chem. Commun.* **2021**, *57*, 10317−10326.

(10) Bhattacharya, S.; Samanta, S. K. Soft-Nanocomposites of Nanoparticles and Nanocarbons with Supramolecular and Polymer Gels and Their Applications. *Chem. Rev.* **2016**, *116*, 11967−12028.

(11) Hirsch, A. *The Chemistry of the Fullerenes*; Thieme: Stuttgart, 1994.

(12) Wróbel, D.; Graja, A. Photoinduced Electron Transfer Processes in Fullerene-Organic Chromophore Systems. *Coord. Chem. Rev.* **2011**, *255*, 2555−2577.

(13) Roncali, J. Molecular Bulk Heterojunctions: An Emerging Approach to Organic Solar Cells. *Acc. Chem. Res.* **2009**, *42*, 1719−1730.

(14) Lin, Y.; Li, Y.; Zhan, X. Small Molecule Semiconductors for High-Efficiency Organic Photovoltaics. *Chem. Soc. Rev.* **2012**, *41*, 4245−4272.

(15) Śliwa, W. Diels-Alder Reactions of Fullerenes. *Fuller. Sci. Technol.* **1997**, *5*, 1133−1175.

(16) Kräutler, B.; Maynollo, J. Diels-Alder Reactions of the [60]Fullerene Functionalizing a Carbon Sphere with Flexibly and with Rigidly Bound Addends. *Tetrahedron* **1996**, *52*, 5033−5042.

(17) Tagmatarchis, N.; Prato, M. The Addition of Azomethine Ylides to [60]Fullerene Leading to Fulleropyrrolidines. *Synlett* **2003**, *2003*, 768−779.

(18) Diederich, F.; Isaacs, L.; Philp, D. Syntheses, Structures, and Properties of Methanofullerenes. *Chem. Soc. Rev.* **1994**, *23*, 243−255.

(19) Bingel, C. Cyclopropanierung von Fullerenen. *Chem. Ber.* **1993**, *126*, 1957−1959.

(20) Artigas, A.; Pla-Quintana, A.; Lledó, A.; Roglans, A.; Solà, M. Expeditious Preparation of Open-Cage Fullerenes by Rhodium(I)-Catalyzed [2+2+2] Cycloaddition of Diynes and C_{60}: An Experimental and Theoretical Study. *Chem. - Eur. J.* **2018**, *24*, 10653−10661.

(21) Su, Y. T.; Wang, Y. L.; Wang, G. W. Palladium-Catalyzed Heteroannulation of [60]Fullerene with N-(2-Arylethyl) Sulfonamides via C-H Bond Activation. *Org. Chem. Front.* **2014**, *1*, 689−693.

(22) Maroto, E. E.; Filippone, S.; Martín-Domenech, A.; Suarez, M.; Martín, N. Switching the Stereoselectivity: (Fullero)Pyrrolidines "a La Carte". *J. Am. Chem. Soc.* **2012**, *134*, 12936−12938.

(23) Solà, M.; Mestres, J.; Martí, J.; Duran, M. An AM1 Study of the Reactivity of Buckminsterfullerene (C_{60}) in a Diels-Alder Model Reaction. *Chem. Phys. Lett.* **1994**, *231*, 325−330.

(24) Fernández, I.; Solà, M.; Bickelhaupt, F. M. Why Do Cycloaddition Reactions Involving C_{60} Prefer [6,6] over [5,6] Bonds? *Chem. - Eur. J.* **2013**, *19*, 7416−7422.

(25) Zhao, P.; Hu, S.; Lu, X.; Zhao, X. Diels-Alder Cycloaddition on Nonisolated-Pentagon-Rule C_{2v}(19138)-C_{76} and YNC@C_{2v}(19138)-C_{76}: The Difference in Regioselectivity Caused by the Inner Metallic Cluster. *J. Org. Chem.* **2019**, *84*, 14571−14578.
(26) Osuna, S.; Swart, M.; Solà, M. The Diels-Alder Reaction on Endohedral $Y_3N@C_{78}$: The Importance of the Fullerene Strain Energy. *J. Am. Chem. Soc.* **2009**, *131*, 129−139.
(27) Osuna, S.; Swart, M.; Solà, M. The Reactivity of Endohedral Fullerenes. What Can Be Learnt from Computational Studies? *Phys. Chem. Chem. Phys.* **2011**, *13*, 3585−3603.
(28) Garcia-Borràs, M.; Osuna, S.; Luis, J. M.; Swart, M.; Solà, M. The Exohedral Diels-Alder Reactivity of the Titanium Carbide Endohedral Metallofullerene $Ti_2C_2@D_{3h}$-C_{78}: Comparison with D_{3h}-C_{78} and $M_3N@D_{3h}$-C_{78} (M=Sc and Y) Reactivity. *Chem. - Eur. J.* **2012**, *18*, 7141−7154.
(29) Garcia-Borràs, M.; Osuna, S.; Luis, J. M.; Swart, M.; Solà, M. The Role of Aromaticity in Determining the Molecular Structure and Reactivity of (Endohedral Metallo)Fullerenes. *Chem. Soc. Rev.* **2014**, *43*, 5089−5105.
(30) Hirsch, A.; Lamparth, I.; Grösser, T.; Karfunkel, H. R. Regiochemistry of Multiple Additions to the Fullerene Core: Synthesis of a T_h-Symmetric Hexakisadduct of C_{60} with Bis-(Ethoxycarbonyl)Methylene. *J. Am. Chem. Soc.* **1994**, *116*, 9385−9386.
(31) Schwenninger, R.; Muller, T.; Krautler, B. Concise Route to Symmetric Multiadducts of [60]Fullerene: Preparation of an Equatorial Tetraadduct by Orthogonal Transposition. *J. Am. Chem. Soc.* **1997**, *119*, 9317−9318.
(32) Lamparth, I.; Maichle−Mössmer, C.; Hirsch, A. Reversible Template-Directed Activation of Equatorial Double Bonds of the Fullerene Framework: Regioselective Direct Synthesis, Crystal Structure, and Aromatic Properties of T_h-$C_{66}(COOEt)_{12}$. *Angew. Chem., Int. Ed.* **1995**, *34*, 1607−1609.
(33) Kräutler, B.; Müller, T.; Maynollo, J.; Gruber, K.; Kratky, C.; Ochsenbein, P.; Schwarzenbach, D.; Bürgi, H. B. A Topochemically Controlled, Regiospecific Fullerene Bisfunctionalization. *Angew. Chem., Int. Ed.* **1996**, *35*, 1204−1206.
(34) Qian, W.; Rubin, Y. Complete Control over Addend Permutation at All Six Pseudooctahedral Positions of Fullerene C_{60}. *J. Am. Chem. Soc.* **2000**, *122*, 9564−9565.
(35) Wang, G. W.; Saunders, M.; Cross, R. J. Reversible Diels - Alder Addition to Fullerenes: A Study of Equilibria Using ^{3}He NMR Spectroscopy. *J. Am. Chem. Soc.* **2001**, *123*, 256−259.
(36) Solà, M.; Duran, M.; Mestres, J. Theoretical Study of the Regioselectivity of Successive 1,3-Butadiene Diels-Alder Cycloadditions to C_{60}. *J. Am. Chem. Soc.* **1996**, *118*, 8920−8924.
(37) Ash, T.; Banerjee, S.; Debnath, T.; Das, A. K. Computational Insights into the Multi-Diels−Alder Reactions of Neutral C_{60} and Its Li^+ Encapsulated Analogue: A Density Functional Theory Study. *Int. J. Quantum Chem.* **2022**, *122*, No. e26824.
(38) Hermann, M.; Wassy, D.; Esser, B. Conjugated Nanohoops Incorporating Donor, Acceptor, Hetero- or Polycyclic Aromatics. *Angew. Chem., Int. Ed.* **2021**, *60*, 15743−15766.
(39) Xu, Y.; von Delius, M. The Supramolecular Chemistry of Strained Carbon Nanohoops. *Angew. Chem., Int. Ed.* **2020**, *59*, 559−573.
(40) Cheung, K. Y.; Segawa, Y.; Itami, K. Synthetic Strategies of Carbon Nanobelts and Related Belt-Shaped Polycyclic Aromatic Hydrocarbons. *Chem. - Eur. J.* **2020**, *26*, 14791−14801.
(41) González-Veloso, I.; Cabaleiro-Lago, E. M.; Rodríguez-Otero, J. Fullerene Size Controls the Selective Complexation of [11]CPP with Pristine and Endohedral Fullerenes. *Phys. Chem. Chem. Phys.* **2018**, *20*, 11347−11358.
(42) Minameyer, M. B.; Xu, Y.; Frühwald, S.; Görling, A.; von Delius, M.; Drewello, T. Investigation of Cycloparaphenylenes (CPPs) and Their Noncovalent Ring-in-Ring and Fullerene-in-Ring Complexes by (Matrix-Assisted) Laser Desorption/Ionization and Density Functional Theory. *Chem. - Eur. J.* **2020**, *26*, 8729−8741.
(43) Iwamoto, T.; Watanabe, Y.; Sadahiro, T.; Haino, T.; Yamago, S. Size-Selective Encapsulation of C_{60} by [10]Cycloparaphenylene: Formation of the Shortest Fullerene-Peapod. *Angew. Chem., Int. Ed.* **2011**, *50*, 8342−8344.
(44) Iwamoto, T.; Watanabe, Y.; Takaya, H.; Haino, T.; Yasuda, N.; Yamago, S. Size- and Orientation-Selective Encapsulation of C_{70} by Cycloparaphenylenes. *Chem. - Eur. J.* **2013**, *19*, 14061−14068.
(45) Stasyuk, A. J.; Stasyuk, O. A.; Solà, M.; Voityuk, A. A. Hypsochromic Solvent Shift of the Charge Separation Band in Ionic Donor-Acceptor $Li^+@C_{60}$⊂[10]CPP. *Chem. Commun.* **2019**, *55*, 11195−11198.
(46) Rio, J.; Beeck, S.; Rotas, G.; Ahles, S.; Jacquemin, D.; Tagmatarchis, N.; Ewels, C.; Wegner, H. A. Electronic Communication between Two [10]Cycloparaphenylenes and Bis(Azafullerene) $(C_{59}N)_2$ Induced by Cooperative Complexation. *Angew. Chem., Int. Ed.* **2018**, *57*, 6930−6934.
(47) Xu, Y.; Kaur, R.; Wang, B.; Minameyer, M. B.; Gsänger, S.; Meyer, B.; Drewello, T.; Guldi, D. M.; Von Delius, M. Concave-Convex π-π Template Approach Enables the Synthesis of [10]-Cycloparaphenylene-Fullerene [2]Rotaxanes. *J. Am. Chem. Soc.* **2018**, *140*, 13413−13420.
(48) Zhan, L.; Dai, C.; Zhang, G.; Zhu, J.; Zhang, S.; Wang, H.; Zeng, Y.; Tung, C.-H.; Wu, L.-Z.; Cong, H. A Conjugated Figure-of-eight Oligoparaphenylene Nanohoop with Adaptive Cavities Derived from Cyclooctatetrathiophene Core. *Angew. Chem., Int. Ed.* **2022**, *61*, No. e202113334.
(49) Ubasart, E.; Borodin, O.; Fuertes-Espinosa, C.; Xu, Y.; García-Simón, C.; Gómez, L.; Juanhuix, J.; Gándara, F.; Imaz, I.; Maspoch, D.; von Delius, M.; Ribas, X. A Three-Shell Supramolecular Complex Enables the Symmetry-Mismatched Chemo- and Regioselective Bis-Functionalization of C_{60}. *Nat. Chem.* **2021**, *13*, 420−427.
(50) Fuertes-Espinosa, C.; Pujals, M.; Ribas, X. Supramolecular Purification and Regioselective Functionalization of Fullerenes and Endohedral Metallofullerenes. *Chem* **2020**, *6*, 3219−3262.
(51) Xu, Y.; Kaur, R.; Wang, B.; Minameyer, M. B.; Gsänger, S.; Meyer, B.; Drewello, T.; Guldi, D. M.; Von Delius, M. Concave-Convex π-π Template Approach Enables the Synthesis of [10]-Cycloparaphenylene-Fullerene [2]Rotaxanes. *J. Am. Chem. Soc.* **2018**, *140*, 13413−13420.
(52) Pang, L. S. K.; Wilson, M. A. Reactions of C_{60} and C_{70} with Cyclopentadiene. *J. Phys. Chem. A* **1993**, *97*, 6761−6763.
(53) Giovane, L. M.; Barco, J. W.; Yadav, T.; Lafleur, A. L.; Marr, J. A.; Howard, J. B.; Rotello, V. M. Kinetic Stability of the C_{60}-Cyclopentadiene Diels-Alder Adduct. *J. Phys. Chem. B* **1993**, *97*, 8560−8561.
(54) Ueno, H.; Kawakami, H.; Nakagawa, K.; Okada, H.; Ikuma, N.; Aoyagi, S.; Kokubo, K.; Matsuo, Y.; Oshima, T. Kinetic Study of the Diels-Alder Reaction of $Li^+@C_{60}$ with Cyclohexadiene: Greatly Increased Reaction Rate by Encapsulated Li^+. *J. Am. Chem. Soc.* **2014**, *136*, 11162−11167.
(55) Frisch, M. J.; Trucks, G. W.; Schlegel, H. B.; Scuseria, G. E.; Robb, M. A.; Cheeseman, J. R.; Scalmani, G.; Barone, V.; Petersson, G. A.; Nakatsuji, H.; Li, X.; Caricato, M.; Marenich, A. V.; Bloino, J.; Janesko, B. G.; Gomperts, R.; Mennucci, B.; Hratchian, H. P.; Ortiz, J. V.; Izmaylov, A. F.; Sonnenberg, J. L.; Williams; Ding, F.; Lipparini, F.; Egidi, F.; Goings, J.; Peng, B.; Petrone, A.; Henderson, T.; Ranasinghe, D.; Zakrzewski, V. G.; Gao, J.; Rega, N.; Zheng, G.; Liang, W.; Hada, M.; Ehara, M.; Toyota, K.; Fukuda, R.; Hasegawa, J.; Ishida, M.; Nakajima, T.; Honda, Y.; Kitao, O.; Nakai, H.; Vreven, T.; Throssell, K.; Montgomery, J. A., Jr; Peralta, J. E.; Ogliaro, F.; Bearpark, M. J.; Heyd, J. J.; Brothers, E. N.; Kudin, K. N.; Staroverov, V. N.; Keith, T. A.; Kobayashi, R.; Normand, J.; Raghavachari, K.; Rendell, A. P.; Burant, J. C.; Iyengar, S. S.; Tomasi, J.; Cossi, M.; Millam, J. M.; Klene, M.; Adamo, C.; Cammi, R.; Ochterski, J. W.; Martin, R. L.; Morokuma, K.; Farkas, O.; Foresman, J. B.; Fox, D. J. *Gaussian 16*, revision C.01; Gaussian, Inc.: Wallingford, CT, 2016.
(56) Becke, A. D. Density-Functional Thermochemistry. III. The Role of Exact Exchange. *J. Chem. Phys.* **1993**, *98*, 5648−5652.

https://doi.org/10.1021/acs.joc.1c03116
J. Org. Chem. 2022, 87, 5149−5157

(57) Lee, C.; Yang, W.; Parr, R. G. Development of the Colle-Salvetti Correlation-Energy Formula into a Functional of the Electron Density. *Phys. Rev. B* **1988**, *37*, 785−789.
(58) Vosko, S. H.; Wilk, L.; Nusair, M. Accurate Spin-Dependent Electron Liquid Correlation Energies for Local Spin Density Calculations: A Critical Analysis. *Can. J. Phys.* **1980**, *58*, 1200−1211.
(59) Stephens, P. J.; Devlin, F. J.; Chabalowski, C. F.; Frisch, M. J. Ab Initio Calculation of Vibrational Absorption and Circular Dichroism Spectra Using Density Functional Force Fields. *J. Phys. Chem. V* **1994**, *98*, 11623−11627.
(60) Ditchfield, R.; Hehre, W. J.; Pople, J. A. Self-Consistent Molecular-Orbital Methods. IX. An Extended Gaussian-Type Basis for Molecular-Orbital Studies of Organic Molecules. *J. Chem. Phys.* **1971**, *54*, 724−728.
(61) Grimme, S.; Ehrlich, S.; Goerigk, L. Effect of the Damping Function in Dispersion Corrected Density Functional Theory. *J. Comput. Chem.* **2011**, *32*, 1456−1465.
(62) Osuna, S.; Swart, M.; Solà, M. Dispersion Corrections Essential for the Study of Chemical Reactivity in Fullerenes. *J. Phys. Chem. A* **2011**, *115*, 3491−3496.
(63) Krishnan, R.; Binkley, J. S.; Seeger, R.; Pople, J. A. Self-Consistent Molecular Orbital Methods. XX. A Basis Set for Correlated Wave Functions. *J. Chem. Phys.* **1980**, *72*, 650−654.
(64) Barone, V.; Cossi, M. Quantum Calculation of Molecular Energies and Energy Gradients in Solution by a Conductor Solvent Model. *J. Phys. Chem. A* **1998**, *102*, 1995−2001.
(65) Tomasi, J.; Persico, M. Molecular Interactions in Solution: An Overview of Methods Based on Continuous Distributions of the Solvent. *Chem. Rev.* **1994**, *94*, 2027−2094.
(66) Zhao, Y.; Truhlar, D. G. Density Functionals with Broad Applicability in Chemistry. *Acc. Chem. Res.* **2008**, *41*, 157−167.
(67) Goerigk, L.; Grimme, S. A Thorough Benchmark of Density Functional Methods for General Main Group Thermochemistry, Kinetics, and Noncovalent Interactions. *Phys. Chem. Chem. Phys.* **2011**, *13*, 6670−6688.

https://doi.org/10.1021/acs.joc.1c03116
J. Org. Chem. 2022, 87, 5149−5157